

Magnetic behavior in a series of cerium ternary intermetallics: Ce_2T_2In ($T=Ni, Cu, Rh, Pd, Pt, \text{ and } Au$)

D. Kaczorowski*

*W. Trzebiatowski Institute for Low Temperature and Structure Research, Polish Academy of Sciences,
 P.O. Box 937, 50-950 Wrocław, Poland
 and Institut für Physikalische Chemie, Universität Wien, Währingerstraße 42, A-1090 Wien, Austria*

P. Rogl and K. Hiebl

*Institut für Physikalische Chemie, Universität Wien, Währingerstraße 42, A-1090 Wien, Austria
 (Received 14 February 1996; revised manuscript received 2 May 1996)*

A group of ternary cerium compounds Ce_2T_2In ($T=Ni, Cu, Rh, Pd, Pt, \text{ and } Au$) has been synthesized. As found from single-crystal and powder x-ray-diffraction studies, all these phases crystallize in a primitive tetragonal structure of the Mo_2FeB_2 type. Magnetic measurements (magnetization, dc and ac susceptibility) have revealed the physical properties of these intermetallics to be mainly governed by the $4f-d$ hybridization. Depending on the filling of the transition metal d band the ground state in Ce_2T_2In changes from a nonmagnetic to a well localized magnetic regime. It was proved that Ce_2Ni_2In and Ce_2Rh_2In are intermediate-valence systems, Ce_2Pt_2In is a strongly temperature-dependent paramagnet, whereas Ce_2Cu_2In , Ce_2Pd_2In , and Ce_2Au_2In order magnetically at low temperatures. Measurements of the electrical resistivity have corroborated the intermediate-valence behavior in Ce_2Ni_2In and Ce_2Rh_2In . In turn, the resistivity of the remaining ternaries studied was found to be determined by an interplay of Kondo scattering and crystal-field effects. For Ce_2Pt_2In which behaves like a spin-fluctuating system due to strong Kondo-type interactions a nonmagnetic heavy-fermion ground state probably occurs. [S0163-1829(96)08134-9]

I. INTRODUCTION

Recently a series of ternary actinoid compounds with the composition An_2T_2M ($An=U, Np$; $T=3d-, 4d-, 5d-$ transition metal; $M=In, Sn$), crystallizing in the tetragonal Mo_2FeB_2 -type structure (an ordered derivative of the U_3Si_2 -type structure), has been discovered.¹⁻³ As a result of intensive experimental²⁻⁸ and theoretical⁹⁻¹² studies of these materials it was established that their electronic properties are mainly determined by the hybridization of the $5f$ states with the d states of transition elements. As for many other families of light actinoid intermetallics, the behavior in the An_2T_2M compounds was found to change gradually from a nonmagnetic to a magnetic ground state when moving from the left to the right of a transition-metal row.^{7,13} Interestingly, most of the uranium 2:2:1 phases exhibit at low temperatures a strong enhancement in the electronic coefficient of the specific heat (γ values up to 830 mJ/mole K^2 as observed for U_2Pt_2In ⁵) and this feature in conjunction with the characteristic magnetic and electrical properties of these compounds may support their classification as heavy-fermion systems.^{5,9,10}

In contrast to the extensively studied actinoid intermetallics with the 2:2:1 stoichiometry only very little is known up to date about the corresponding rare-earth-based materials. This fact has motivated us to start a systematic investigation of the Ce_2T_2In compounds. Our choice of cerium-based phases is due to a common tendency of this element to show anomalous physical behavior in its binary or ternary intermetallics. Although already in 1990 the formation of Ce_2Ni_2In and Ce_2Cu_2In was described by Kalychak *et al.*,¹⁴ the magnetic properties of these two compounds were not studied at that time. More recently Hulliger and Xue¹⁵ synthesized the

Ce_2Pd_2In and found that it is ferromagnetic below $T_c=4$ K. This finding has subsequently been confirmed by Gordon *et al.*¹⁶ who also reported on the nonmagnetic properties of Ce_2Ni_2In . Already in the course of our present study two further publications by Hulliger appeared which addressed the synthesis of Ce_2Pt_2In (Ref. 17) and Ce_2Rh_2In .¹⁸ The first compound was briefly mentioned to be paramagnetic down to 1.5 K (Ref. 17) and for the latter a nonmagnetic ground state was claimed¹⁸ due to the presence of Ce^{4+} ions.

In the present paper we give an extended survey of the physical behavior in the Ce_2T_2In intermetallics with $T=Ni, Cu, Rh, Pd, Pt, \text{ and } Au$. We report here on the crystal structure refinements from x-ray data and present the results of detailed magnetization, dc susceptibility, ac susceptibility, and electrical resistivity measurements performed on polycrystalline samples of Ce_2T_2In . In the discussion we emphasize the role of interactions between the cerium $4f$ electrons and the d electrons of neighboring transition-metal atoms in the magnetic moment formation in the compounds studied.

II. EXPERIMENTAL DETAILS

Polycrystalline samples of La_2T_2In and Ce_2T_2In were prepared by arc melting the appropriate amounts of the constituent elements in a titanium gettered argon atmosphere. The buttons were turned over and remelted several times to ensure a good homogeneity. Weight losses after meltings were always smaller than 0.5 mass%. No further heat treatment was given to the ingots except for Ce_2T_2In , $T=Ni, Rh, Pd$, which were subsequently wrapped with molybdenum foil, sealed in evacuated quartz tubes and annealed at 650 °C for two weeks. All the samples obtained (as cast and annealed)

TABLE I. Lattice parameters and unit-cell volumes for La_2T_2In and Ce_2T_2In compounds refined from the Guinier x-ray data. Standard deviations in the positions of the least significant digits are given in parentheses.

Compound	a (nm)	c (nm)	c/a	V (nm^3)
$\text{La}_2\text{Ni}_2\text{In}$	0.7627(3)	0.3905(1)	0.512	0.2272(2)
$\text{La}_2\text{Cu}_2\text{In}$	0.7964(9)	0.9906(7)	0.512	0.2426(1)
$\text{La}_2\text{Rh}_2\text{In}$	0.7810(9)	0.3943(1)	0.505	0.2405(6)
$\text{La}_2\text{Pd}_2\text{In}$	0.7869(1)	0.3963(1)	0.504	0.2454(1)
$\text{La}_2\text{Pt}_2\text{In}$	0.7881(1)	0.3938(1)	0.500	0.2446(1)
$\text{La}_2\text{Au}_2\text{In}$	0.8099(1)	0.4003(1)	0.494	0.2625(1)
$\text{Ce}_2\text{Ni}_2\text{In}$	0.7528(3)	0.3727(1)	0.495	0.2112(2)
$\text{Ce}_2\text{Cu}_2\text{In}$	0.7735(3)	0.3924(2)	0.507	0.2348(2)
$\text{Ce}_2\text{Rh}_2\text{In}$	0.7591(1)	0.3773(1)	0.497	0.2174(1)
$\text{Ce}_2\text{Pd}_2\text{In}$	0.7793(2)	0.3927(1)	0.504	0.2385(1)
$\text{Ce}_2\text{Pt}_2\text{In}$	0.7808(1)	0.3880(1)	0.497	0.2366(1)
$\text{Ce}_2\text{Au}_2\text{In}$	0.8046(2)	0.3943(1)	0.490	0.2553(1)

were examined by x-ray powder diffraction using a Guinier camera with $\text{Cu } K\alpha_1$ radiation. It appeared that our attempts to synthesize Ce_2T_2In compounds with $T=\text{Fe, Co, Ru, Ag, and Ir}$ have failed. No efforts were made to prepare $\text{Ce}_2\text{Os}_2\text{In}$. With all the other transition metals the La- and Ce-based 2:2:1 phases form easily probably in a congruent manner. The samples of these compounds have a metallic lustre and are stable in air except for $\text{Ce}_2\text{Au}_2\text{In}$ which deteriorates quickly.

Lattice parameters were obtained by least-squares refinements of the Guinier data using 5N germanium as an internal standard. The diffraction lines were identified via intensity calculations¹⁹ using the positional parameters of $\text{Ce}_2\text{Ni}_2\text{In}$ taken from Ref. 14. No extra lines due to impurities and/or superstructure formation [as found for some rare-earth stannides $L_2\text{Au}_2\text{Sn}$ ($L=\text{Y, Dy, Ho, Er, Tm, Lu}$) (Ref. 20) and indides $L_2\text{Au}_2\text{In}$ ($L=\text{Tm, Lu}$) (Ref. 21) as well as for the two uranium compounds $\text{U}_2\text{Pt}_2\text{Sn}$ (Ref. 22) and $\text{U}_2\text{Ir}_2\text{Sn}$ (Ref. 23)] were observed. The lattice parameters determined for La_2T_2In and Ce_2T_2In compounds with $T=\text{Ni, Cu, Rh, Pd, Pt, and Au}$ are listed in Table I.

A small single-crystal fragment of $\text{Ce}_2\text{Pd}_2\text{In}$ (0.04 mm \times 0.03 mm \times 0.06 mm) was obtained by mechanical fragmentation of the arc melted button with the nominal composition (in at. %) $\text{Ce}_{40}\text{Pd}_{40}\text{In}_{20}$, which was annealed for 240 h at 800 °C in an evacuated quartz capsule. A total number of 3274 x-ray reflections have been recorded on a STOE Nicolet four-circle diffractometer ($\omega/2\theta$ scans) employing an empirical absorption correction [$\mu(\text{Mo } K\alpha)=30.7 \text{ mm}^{-1}$] from psi scans of five independent reflections. The crystallographic data are summarized in Table II. Analyses of Weissenberg photographs (axis [001]) revealed a primitive tetragonal lattice geometry with high tetragonal Laue symmetry and without any indications of superstructure formation. The only sets of extinctions observed were: $(0kl)$ for $k=2n+1$ and $(h00)$ for $h=2n+1$; this observation is consistent with the centrosymmetric type of space group $P4/mbm$ with the highest possible symmetry.

Room-temperature x-ray powder diffraction intensity data for powder structure refinement were obtained from flat samples for Ce_2T_2In , $T=\text{Ni, Cu, Rh, Pt, and Au}$, in a

Siemens D5000 diffractometer with $\text{Cu } K\alpha_1$ radiation and a secondary graphite monochromator. The diffractometer was operated in the step scan mode with $10^\circ \leq 2\theta \leq 120^\circ$, $\Delta\theta = 0.01^\circ$, and a step time of 60–100 s. Rietveld full matrix full profile refinements were performed employing the program FULLPROF.²⁵ In order to prevent progressive decomposition of the finely spread moisture sensitive powders during the time of x-ray exposure, a thinly sprayed-on protective layer of hair spray was applied.

Magnetization and dc magnetic-susceptibility measurements were performed on polycrystalline samples of Ce_2T_2In in the temperature interval 1.7–300 K and in applied magnetic fields up to 50 kOe using a Quantum Design MPMS-5 superconducting quantum interference device magnetometer. For $\text{Ce}_2\text{Rh}_2\text{In}$ and $\text{Ce}_2\text{Ni}_2\text{In}$ the susceptibility measurements were extended up to 900 K employing a pendulum magnetometer SUS 10. The dynamical magnetic susceptibility of $\text{Ce}_2\text{Cu}_2\text{In}$ was determined using a Lake Shore ac susceptometer. Electrical resistivity measurements were carried out on both as-cast and annealed bar-shaped specimens of La_2T_2In and Ce_2T_2In in the temperature range 4.5–300 K by the conventional ac four-probe technique.

III. RESULTS AND DISCUSSION

A. Crystal structure

The positional and isotropic thermal parameters for $\text{Ce}_2\text{Pd}_2\text{In}$, as derived from a single-crystal study, are listed in Table II. The anisotropic thermal parameters and structure factor tables are available on request. The positional parameters for the remaining compounds, Ce_2T_2In , obtained from Rietveld refinements²⁵ are also presented in Table II including the distances between nearest-neighbor atoms.

The crystal structure of the Ce_2T_2In compounds, shown in Fig. 1, in all cases investigated is isotypic with the ordered U_3Si_2 -type structure, where the one U site (Ce site) is replaced by the In atom, thereby adopting the atom order as observed in the Mo_2FeB_2 -type. It is interesting to note that this replacement virtually decreases the coordination number of the In atom, as far as the In-In contacts in direction [001] are concerned. While these distances in U_3Si_2 are bonding distances for the much larger uranium atoms (CN=14), they significantly exceed the sum of the In-metal radii resulting in a mere CN=12 for the In site. As is apparent from Table I and Table II, the unit-cell dimensions of the Ce_2T_2In compounds do not scale with the atomic sizes of the constituent transition elements. For example, the radii of Rh and Pd atoms are rather similar but the difference between the unit-cell volume of $\text{Ce}_2\text{Rh}_2\text{In}$ and that of $\text{Ce}_2\text{Pd}_2\text{In}$ is enormous. In turn, the unit cell of $\text{Ce}_2\text{Rh}_2\text{In}$ has almost the same dimensions as that of $\text{Ce}_2\text{Ni}_2\text{In}$ despite the very significant difference in the radii of rhodium and nickel atoms. Hence, the observed variation in the lattice parameters of the Ce_2T_2In phases is supposed to have mainly an electronic origin and thus the interatomic distances within the 2:2:1 series reflect dominant features in the bonding between cerium and transition metal atoms and between the T -metal atom pairs. Indeed, the unit cells of those compounds which contain transition metals with completely filled d band, i.e., $\text{Ce}_2\text{Cu}_2\text{In}$, $\text{Ce}_2\text{Pd}_2\text{In}$, and $\text{Ce}_2\text{Au}_2\text{In}$, are significantly larger than the unit cells of $\text{Ce}_2\text{Ni}_2\text{In}$ and $\text{Ce}_2\text{Rh}_2\text{In}$, which are based on transi-

TABLE II. Structural data for Ce_2T_2In compounds; space group $P4/mbm-D_{4h}^5$ (No. 127); origin at center, $Z=2$; Mo_2FeB_2 -type (ordered U_3Si_2 -type); standard deviations in parentheses.

Parameter/Compound	$\text{Ce}_2\text{Ni}_2\text{In}$	$\text{Ce}_2\text{Cu}_2\text{In}$	$\text{Ce}_2\text{Rh}_2\text{In}$	$\text{Ce}_2\text{Pd}_2\text{In}$	$\text{Ce}_2\text{Pt}_2\text{In}$	$\text{Ce}_2\text{Au}_2\text{In}$		
a (nm)	0.75305(3)	0.77368(6)	0.75884(2)	0.7813(4)	0.78048(3)	0.80474(3)		
c (nm)	0.37223(2)	0.39240(3)	0.37709(1)	0.3916(2)	0.38808(2)	0.39407(2)		
V (nm ³)	0.21109	0.23488	0.21714	0.2394	0.23640	0.25520		
ρ_x (Mg m ⁻³) (for $Z=2$, stoichiom)	8.06	7.38	9.19	8.43	11.03	10.27		
Data collection	D5000	D5000	D5000	STOE	D5000	D5000		
Radiation	Cu $K\alpha$	Cu $K\alpha$	Cu $K\alpha$	Mo $K\alpha$	Cu $K\alpha$	Cu $K\alpha$		
Reflections measured	149	160	154	441 [$>3\sigma(I_0)$]	160	171		
Θ range	$20 \leq 2\Theta \leq 100$	$20 \leq 2\Theta \leq 100$	$20 \leq 2\Theta \leq 100$	$2 \leq 2\Theta \leq 80$	$20 \leq 2\Theta \leq 100$	$20 \leq 2\Theta \leq 100$		
Refinement	Rietveld	Rietveld	Rietveld	SHELX 76	Rietveld	Rietveld		
Number of variables	20	20	20	14	20	20		
$R_F = \sum F_0 - F_c / \sum F_0$	0.063	0.050	0.053	0.028	0.064	0.065		
$R_I = \sum I_{0B} - I_{cB} / \sum I_{0B}$	0.078	0.074	0.076		0.097	0.078		
$R_{wP} = [\sum w_i y_{0i} - y_{ci} ^2 / \sum w_i y_{0i} ^2]^{1/2}$	0.164	0.147	0.135	0.020 ^a	0.187	0.120		
$R_P = \sum y_{0i} - y_{ci} / \sum y_{0i} $	0.127	0.107	0.107		0.141	0.099		
$R_e = [(N - P + C) / (\sum w_i y_{0i}^2)]^{1/2}$	0.067	0.033	0.069	0.045	0.076	0.057		
$S = R_{wP} / R_e$; $\chi^2 = (R_{wP} / R_e)^2$	$\chi^2 = 5.75$	$\chi^2 = 5.05$	$\chi^2 = 3.78$	$S = 4.25$	$\chi^2 = 6.14$	$\chi^2 = 4.92$		
Atom parameters ^b								
Ce in $4h$ ($x, 1/2 + x, 1/2$)								
x	0.6741(2)	0.6798(1)	0.6714(2)	0.67589(7)	0.6738(2)	0.6759(2)		
$B_{\text{eq}}(B_{\text{iso}})10^2$ (nm ²)	1.26(5)	0.93(9)	1.28(4)	1.08(2) ^c	0.97(5)	0.59(2)		
occ	0.87(1)	0.90(3)	1.0	1.0	0.98(2)	0.96(1)		
T in $4g$ ($x, 1/2 + x, 0$)								
x	0.1221(4)	0.1177(5)	0.1341(2)	0.1276(1)	0.1300(2)	0.1245(1)		
$B_{\text{eq}}(B_{\text{iso}})10^2$ (nm ²)	2.23	1.14(3)	1.30(6)	1.38(2) ^c	1.34(3)	1.36(5)		
occ	1.0	0.96(1)	1.0	1.0	1.0	1.0		
In in $2a$ (0,0,0)								
$B_{\text{eq}}(B_{\text{iso}})10^2$ (nm ²)	2.15(11)	2.3(2)	1.18(8)	1.42(3) ^c	1.44(7)	1.38(8)		
occ	1.0	1.0	1.0	1.0	1.0	1.0		
Distances (nm) within the first nearest-neighbor coordination								
Ce	-4 Ce	CN=17	0.3935	0.4018	0.3977	0.4075	0.4080	0.4197
	-2 Ce		0.3722	0.3924	0.3771	0.3916	0.3881	0.3941
	-1 Ce		0.3708	0.3937	0.3679	0.3887	0.3837	0.4004
	-4 In		0.3348	0.3453	0.3386	0.3485	0.3477	0.3562
	-4 T		0.2931	0.3064	0.3002	0.3100	0.3083	0.3146
T	-2 T		0.2859	0.2957	0.2813	0.2925	0.2908	0.3007
	-4 Ce	CN=9	0.2931	0.3064	0.3002	0.3100	0.3083	0.3146
	-2 In		0.2991	0.3094	0.2957	0.3075	0.3061	0.3184
	-1 T		0.2601	0.2580	0.2878	0.2821	0.2870	0.2834
-2 Ce	0.2859		0.2957	0.2813	0.2926	0.2908	0.3007	
In	-8 Ce	CN=12	0.3348	0.3453	0.3386	0.3485	0.3477	0.3562
	-4 T		0.2991	0.3094	0.2957	0.3075	0.3061	0.3184

^aWeighting function: $w_i = 2.5874 / [\sigma^2(F) + 0.0001 \times F^2]$; secondary extinction parameter: $g = 0.0022(1)$ [SHELX-76, Ref. (24)].

^bStandardized set of atom parameters using program STRUCTURE TIDY-TYPIX (Ref. 26).

^c $U_{\text{iso}} \sim U_{\text{equiv}}$; a list of anisotropic temperature parameters can be obtained on request.

tion metals with d^8 -atomic configuration. As a consequence, the $4f$ electrons in the two latter compounds apparently contribute to the bonding and the f - d hybridization is there quite strong (see magnetism).

A detailed description of the crystal structure of the Mo_2FeB_2 -type can be found in the literature.^{1-3,15} We recall

here only that the unit cell of the Ce_2T_2In intermetallics exhibits a typical layered character being composed of two different alternating atomic planes: one containing only cerium atoms and the other with indium and transition-metal atoms. Each of four equivalent cerium atoms in the unit cell has two Ce neighbors along the c axis and one Ce neighbor in the

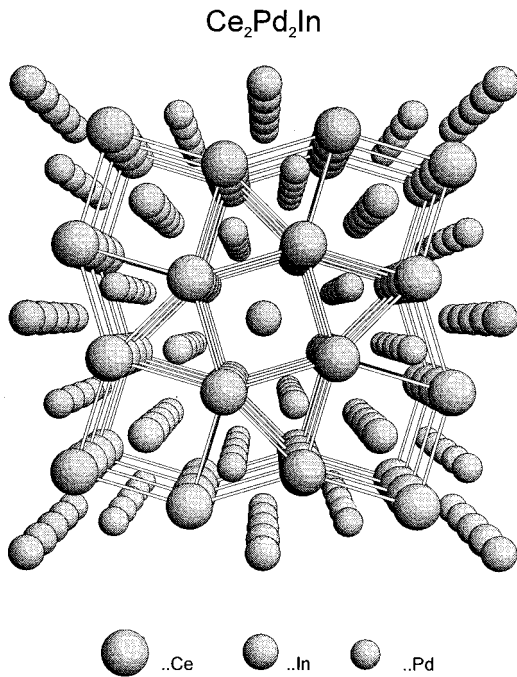


FIG. 1. Perspective view along the c axis of the crystal structure of $\text{Ce}_2\text{Pd}_2\text{In}$.

basal plane (the next-nearest four cerium neighbors are also located in the basal plane, see Fig. 1). Both these distances are very close to one another and only tiny structural details decide which of them is shorter. As seen from Table II in the case of $\text{Ce}_2\text{Cu}_2\text{In}$ and $\text{Ce}_2\text{Au}_2\text{In}$ the Ce-Ce nearest neighbors are along the tetragonal axis, while for the remaining compounds they lie within the basal plane. The cerium atoms are located at the sites of the C_2 -point symmetry and each of them has the C_2 axis rotated by about $\pi/2$ with respect to that of its nearest neighbors. Thus, having in mind that the magnetic moments are usually aligned along the directions of the highest multiplicity, one can expect the formation in the Ce_2T_2In compounds of complex noncollinear magnetic structures associated with the cerium atom sublattices. This feature is probably also responsible for canted uranium moment arrangements determined recently for $\text{U}_2\text{Pd}_2\text{In}$ and $\text{U}_2\text{Pd}_2\text{Sn}$ (Ref. 6) as well as for $\text{U}_2\text{Ni}_2\text{In}$ (Ref. 8).

B. Magnetic properties

$\text{Ce}_2\text{Ni}_2\text{In}$ and $\text{Ce}_2\text{Rh}_2\text{In}$

The temperature variations of the magnetic susceptibility for $\text{Ce}_2\text{Ni}_2\text{In}$ and $\text{Ce}_2\text{Rh}_2\text{In}$, measured up to 900 K, are shown in Fig. 2. In agreement with previously published results^{16,18} the susceptibility of these two compounds is small (of the order of 10^{-3} emu/mole Ce atom) and only weakly temperature dependent. The overall shape of these $\chi(T)$ curves with characteristic broad maxima occurring at elevated temperatures is reminiscent of intermediate-valence (IV) systems. However, at the lowest temperatures, the susceptibility rises with decreasing temperature instead of tending to a constant value as could be expected for IV compounds. Such a low-temperature tail in $\chi(T)$ is frequently observed for cerium-based materials and commonly attrib-

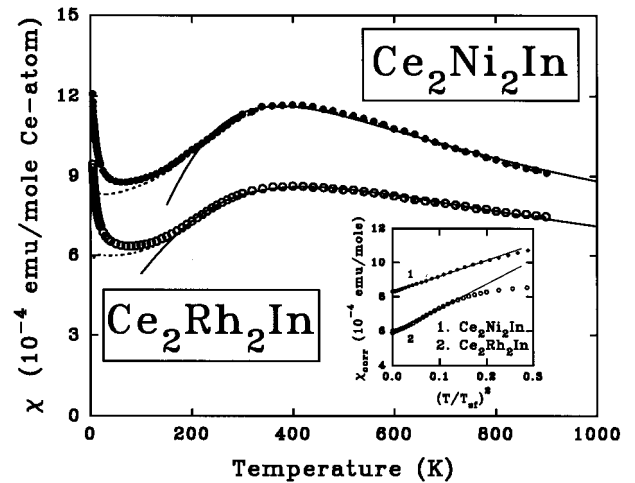


FIG. 2. Temperature dependence of the magnetic susceptibility for $\text{Ce}_2\text{Ni}_2\text{In}$ (filled symbols) and $\text{Ce}_2\text{Rh}_2\text{In}$ (open symbols). The dashed lines denote the corrected data (see text). The solid lines are least-squares fits of $\chi(T)$ according to the ICF model. The inset presents the corrected susceptibility vs $(T/T_{\text{sf}})^2$ where T_{sf} is the appropriate spin-fluctuation temperature. The solid lines in the inset are fits of the experimental data to Eq. (2).

uted to the presence of small amounts of foreign impurities, oxides of cerium, etc.²⁷⁻²⁹ To account for this impurity contribution we followed the procedure employed by Béal-Monod and Lawrence.²⁷ Neglecting crystal-field effects on impurity sites, we assumed that at sufficiently low temperatures the measured susceptibility can be expressed as

$$\chi(T \rightarrow 0) = \chi(0) + \frac{C_{\text{imp}}}{T}, \quad (1)$$

where $\chi(0)$ denotes the intrinsic susceptibility of a IV compound at $T=0$ K, and C_{imp} is the Curie constant of impurity magnetic moments. Moreover, if the impurity contribution is composed only of stable Ce^{3+} ions, one can define the impurity concentration $n = C_{\text{imp}}/C$, where $C = 0.807$ emu/mole K is the Curie constant of free Ce^{3+} ions. Fitting the experimental data of $\text{Ce}_2\text{Ni}_2\text{In}$ for $T < 50$ K to Eq. (1) yielded the parameters: $\chi(0) = 8.32 \times 10^{-4}$ emu/mole Ce atom and $n = 5.5 \times 10^{-3}$ Ce atom/mole, and for $\text{Ce}_2\text{Rh}_2\text{In}$: $\chi(0) = 6.01 \times 10^{-4}$ emu/mole Ce atom and $n = 5.3 \times 10^{-3}$ Ce atom/mole. Finally, the measured $\chi(T)$ dependences were corrected for impurities subtracting the term nC/T from the experimental data in the whole temperature region studied. The so-corrected $\chi(T)$ curves are displayed in Fig. 2 by dashed lines.

According to the paramagnon model of IV materials developed by Béal-Monod and Lawrence²⁷ the magnetic susceptibility varies at low temperatures as

$$\chi(T) = \chi(0) \left[1 + a \left(\frac{T}{T_{\text{sf}}} \right)^2 \right], \quad (2)$$

where a is a positive number of order unity and T_{sf} denotes a characteristic temperature related to spin fluctuations which is given by

$$T_{sf} = \frac{C}{2\chi(0)}. \quad (3)$$

For $\text{Ce}_2\text{Ni}_2\text{In}$ and $\text{Ce}_2\text{Rh}_2\text{In}$ the spin-fluctuation temperature found from Eq. (3) is very high and amounts to 485 and 672 K, respectively. These values are consistent with the prediction offered by Lawrence, Riseborough and Parks²⁹

$$T_{sf} = \frac{3}{2} T(\chi^{\max}) \quad (4)$$

relating T_{sf} to the temperature where the susceptibility exhibits a maximum [the magnitude of $T(\chi^{\max})$ found from Fig. 2 is about 375 and 410 K for $\text{Ce}_2\text{Ni}_2\text{In}$ and $\text{Ce}_2\text{Rh}_2\text{In}$, respectively]. In the inset to Fig. 2 the corrected susceptibility data for $\text{Ce}_2\text{Ni}_2\text{In}$ and $\text{Ce}_2\text{Rh}_2\text{In}$ plotted versus $(T/T_{sf})^2$ are shown together with their fits to Eq. (2). It appears that for both compounds the theory by Béal-Monod and Lawrence²⁷ works well up to about 200 K. The slopes of the theoretical lines amount to 1.06 and 0.98 for the Ni- and Rh-containing phase, respectively, and the extrapolated intercepts give the $\chi(0)$ values equal to those derived above.

An alternative approach describing the features of intermediate-valence systems is the interconfiguration fluctuation (ICF) model developed by Sales and Wohleben.³⁰ In the scope of this model the magnetic susceptibility of a IV cerium compound (with the $4f^0$ ground state) is given by

$$\chi(T) = \frac{N\mu_{\text{eff}}^2[1 - \nu(T)]}{3k_B(T + T_{sf}^*)}, \quad (5)$$

where $\mu_{\text{eff}} = 2.54\mu_B$ is the effective magnetic moment of the cerium $4f^1$ state, T_{sf}^* denotes a characteristic temperature associated with fluctuations between the $4f^0$ and $4f^1$ states due to interactions with conduction electrons, while $\nu(T)$ stands for the mean occupation of the ground state. This fractional valence is temperature and energy dependent via the relation

$$\nu(T) = \frac{1}{1 + 6 \exp[-E_{\text{ex}}/k_B(T + T_{sf}^*)]}, \quad (6)$$

where E_{ex} is the energy difference between the $4f^1$ and $4f^0$ states. The ICF model is frequently modified³¹ adding to Eq. (5) a constant term χ_0 which accounts for possible conduction-electron paramagnetic and core-electron diamagnetic contributions as well as for the temperature-independent Van Vleck contribution to the total measured magnetic susceptibility. It appears that the so-modified ICF model describes well the magnetic behavior in $\text{Ce}_2\text{Rh}_2\text{In}$ and $\text{Ce}_2\text{Ni}_2\text{In}$ observed for $T > 200$ K. The least-squares fits of the experimental $\chi(T)$ variations for both compounds are shown in Fig. 2 by solid lines, and the fitting parameters are as follows: $E_{\text{ex}} = 884$ K, $T_{sf}^* = 92$ K, and $\chi_0 = 3.4 \times 10^{-4}$ emu/mole Ce atom for $\text{Ce}_2\text{Ni}_2\text{In}$, and $E_{\text{ex}} = 1179$ K, $T_{sf}^* = 201$ K, and $\chi_0 = 2.5 \times 10^{-4}$ emu/mole Ce atom for $\text{Ce}_2\text{Rh}_2\text{In}$. Then, from Eq. (6) it is possible to estimate the temperature dependence of the cerium atom valence. Assuming that the highest possible valence for the cerium $4f^0$ state is 3.30 (for discussion, see Ref. 32) one obtains in the temperature region, where the susceptibility for $\text{Ce}_2\text{Rh}_2\text{In}$ and $\text{Ce}_2\text{Ni}_2\text{In}$ obeys the ICF model, a strong decrease in the effective valence from +3.23 at 200 K in both compounds

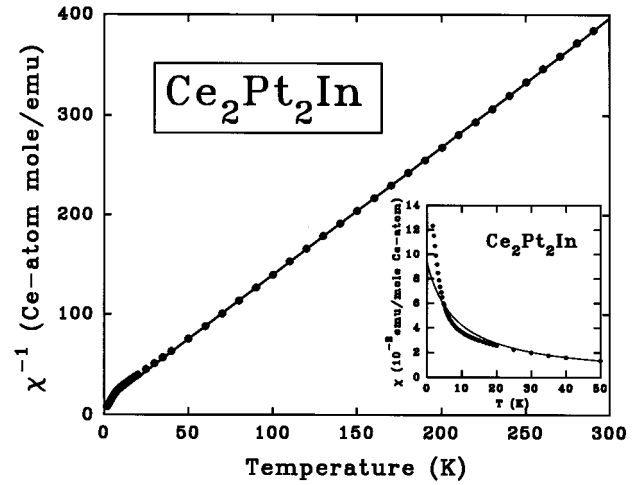


FIG. 3. Temperature variation of the inverse magnetic susceptibility for $\text{Ce}_2\text{Pt}_2\text{In}$. The inset shows the susceptibility of this compound at low temperatures. The solid lines are fits of the experimental data to the Curie-Weiss law.

down to +3.07 and +3.10 at 900 K for the Ni- and Rh-containing phase, respectively.

Finally, it seems worthwhile to compare $\text{Ce}_2\text{Ni}_2\text{In}$ and $\text{Ce}_2\text{Rh}_2\text{In}$ with respect to their magnetic behavior. Both compounds have the nonmagnetic ground state that can be deduced already from the low magnitude of their almost temperature independent susceptibility but also from the very large values of T_{sf} , T_{sf}^* , and E_{ex} derived above as well as from the value of the effective cerium atom valence which at low temperatures is close to that expected for the nonmagnetic $4f^0$ configuration. However, the susceptibility of $\text{Ce}_2\text{Rh}_2\text{In}$ is apparently lower and less temperature dependent than that observed for $\text{Ce}_2\text{Ni}_2\text{In}$. Also the characteristic temperatures obtained for this compound are much higher than those found for the Ni-containing counterpart. Moreover, the excited $4f^1$ state lies lower in energy in $\text{Ce}_2\text{Ni}_2\text{In}$ which is reflected in a slightly faster decrease of the effective valence in this material with increasing temperature. All these findings unambiguously indicate that the interactions between the cerium $4f$ states and the conduction band states are stronger in $\text{Ce}_2\text{Rh}_2\text{In}$ than those in $\text{Ce}_2\text{Ni}_2\text{In}$. This is certainly due to the larger spatial extent of the rhodium $4d$ states in comparison to the nickel $3d$ states causing the f - d hybridization being more effective in the case of $\text{Ce}_2\text{Rh}_2\text{In}$.

$\text{Ce}_2\text{Pt}_2\text{In}$

The $\chi^{-1}(T)$ dependence measured for $\text{Ce}_2\text{Pt}_2\text{In}$ is displayed in Fig. 3. Above 30 K the susceptibility follows the Curie-Weiss law with the effective magnetic moment $\mu_{\text{eff}} = 2.49\mu_B/\text{Ce atom}$ and the paramagnetic Curie temperature $\theta_p = -8.4$ K. This value of μ_{eff} is very close to that expected for a free Ce^{3+} ion [$g\sqrt{j(j+1)} = 2.54$] and indicates a development of well localized magnetic moments in $\text{Ce}_2\text{Pt}_2\text{In}$. Yet, down to 1.7 K no magnetic ordering in this compound is observed in accordance with the results obtained before¹⁵ (see inset to Fig. 3). Below 30 K $\chi^{-1}(T)$ deviates markedly from a straight line behavior presumably due to thermal depopulation of crystal-field split cerium $4f^1$ states.

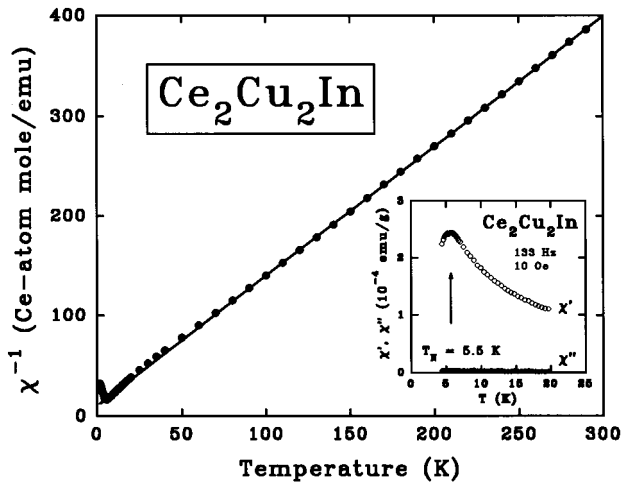


FIG. 4. Temperature variation of the inverse magnetic susceptibility for $\text{Ce}_2\text{Cu}_2\text{In}$. The solid line is a fit of the experimental data to the Curie-Weiss law. The inset shows the complex magnetic susceptibility versus temperature for $\text{Ce}_2\text{Cu}_2\text{In}$ taken in zero external static magnetic field. The arrow marks the Néel temperature.

$\text{Ce}_2\text{Cu}_2\text{In}$ and $\text{Ce}_2\text{Au}_2\text{In}$

Figure 4 shows the magnetic-susceptibility variation for $\text{Ce}_2\text{Cu}_2\text{In}$. A characteristic maximum in $\chi(T)$ strongly suggests that the compound orders antiferromagnetically below $T_N=5.5$ K. This observation is further corroborated by the results of ac magnetic-susceptibility measurements presented in the inset to Fig. 4. As seen from this figure, only the real component of the ac susceptibility exhibits a pronounced maximum at T_N , while the imaginary component remains temperature independent down to 4.5 K. A further argument for an antiferromagnetic ground state in $\text{Ce}_2\text{Cu}_2\text{In}$ comes from the behavior of the magnetization measured at $T=1.7$ K as a function of applied magnetic field. As shown in Fig. 5(a), the magnetization first increases linearly up to about 20 kOe and then shows a pronounced metamagnetic transition. At $H=50$ kOe the magnetization reaches the value of 13.5 emu/g being, however, apparently still far away from magnetic saturation.

In the paramagnetic region the susceptibility of $\text{Ce}_2\text{Cu}_2\text{In}$ obeys a Curie-Weiss law (above 50 K) with the parameters: $\mu_{\text{eff}}=2.48\mu_B/\text{Ce}$ atom and $\theta_p=-7.7$ K. Below 50 K crystal-field effects are likely responsible for deviations of the $\chi^{-1}(T)$ curve from a linear behavior.

Magnetic properties similar to that of $\text{Ce}_2\text{Cu}_2\text{In}$ were also found for $\text{Ce}_2\text{Au}_2\text{In}$ (see Fig. 6). At $T_N=3.2$ K the $\chi(T)$ curve, measured in small magnetic fields, exhibits a pronounced maximum that can be ascribed to an antiferromagnetic phase transition. Yet, as shown in the inset to Fig. 6, the maximum starts to move to lower temperatures and markedly broadens if the strength of magnetic field is increased. This unusual behavior becomes clear when inspecting the field dependence of the magnetization displayed in Fig. 5(b). It appears that in $\text{Ce}_2\text{Au}_2\text{In}$ a metamagnetic transition takes place already above 5 kOe. Obviously this feature makes the susceptibility of the compound taken in $H>H_c$ strongly field dependent. Magnetic saturation is reached at $H_s=30$ kOe, and in stronger magnetic fields the magnetization only slightly rises with increasing field strength presum-

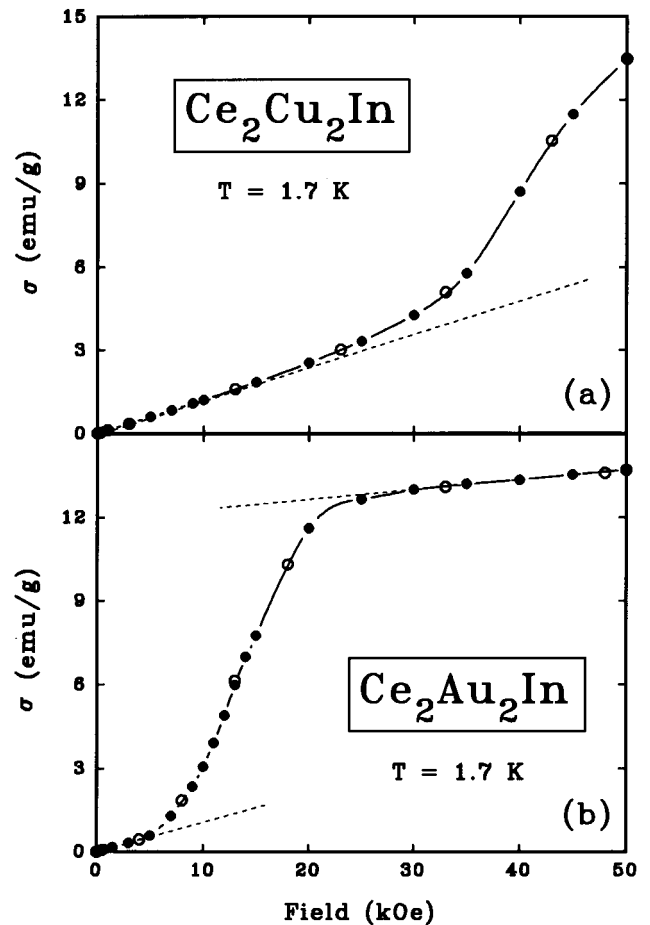


FIG. 5. Field dependence of the magnetization for (a) $\text{Ce}_2\text{Cu}_2\text{In}$ and (b) $\text{Ce}_2\text{Au}_2\text{In}$ measured at 1.7 K with increasing (filled symbols) and decreasing (open symbols) magnetic field. The dashed lines show a straight-line behavior of $\sigma(H)$ observed for $\text{Ce}_2\text{Cu}_2\text{In}$ below about 20 kOe and for $\text{Ce}_2\text{Au}_2\text{In}$ below about 5 and above about 30 kOe.

ably due to a paraprocess effect. The value of σ found in 50 kOe is 13.7 emu/g that corresponds to the magnetic moment of $0.97\mu_B/\text{Ce}$ atom. From the values of H_c , H_s , and $\sigma(50$ kOe) determined for $\text{Ce}_2\text{Au}_2\text{In}$ it can be anticipated that the magnetocrystalline anisotropy in this compound is strongly reduced with respect to that characteristic of $\text{Ce}_2\text{Cu}_2\text{In}$.

For $T>50$ K the fit of $\chi(T)$ to a Curie-Weiss expression yields the effective magnetic moment $\mu_{\text{eff}}=2.48\mu_B/\text{Ce}$ atom and the paramagnetic Curie temperature $\theta_p=-15.7$ K. A distinct downward curvature of $\chi^{-1}(T)$, observed below 50 K, presumably results from strong crystal-field interactions.

$\text{Ce}_2\text{Pd}_2\text{In}$

From the magnetic behavior of $\text{Ce}_2\text{Pd}_2\text{In}$, presented in Fig. 7, it is clear that the ground state in this compound is ferromagnetic, in accordance with the results published before.^{15,16} It appears that the Pd-containing phase is the only ferromagnetic representative of the $\text{Ce}_2\text{T}_2\text{In}$ family and one of very few ferromagnets among the rare-earth-based 2:2:1 intermetallics.¹⁶⁻¹⁸ Interestingly enough is that up to date no ferromagnetically ordered actinide-based 2:2:1 materials have been found.^{7,13}

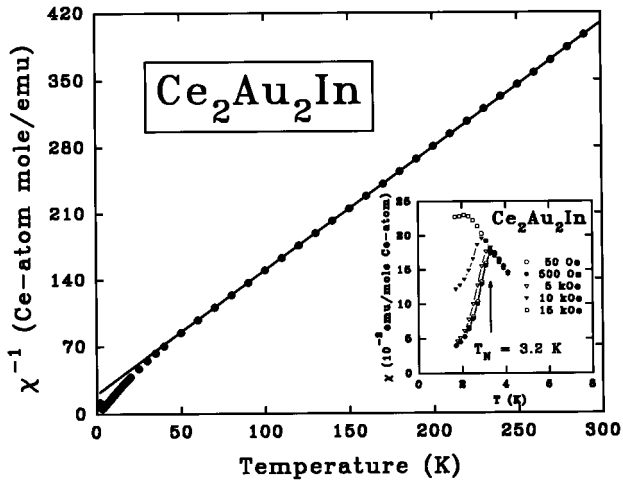


FIG. 6. Temperature variation of the inverse magnetic susceptibility for $\text{Ce}_2\text{Au}_2\text{In}$. The solid line is a fit of the experimental data to the Curie-Weiss law. The inset displays the susceptibility of this compound at low temperatures taken in several magnetic fields. The solid lines in the inset serve as a guide for the eye, and the arrow marks the ordering temperature.

The $\sigma(H)$ curve for $\text{Ce}_2\text{Pd}_2\text{In}$ (see the inset to Fig. 7) saturates already above 5 kOe indicating a rather weak magnetocrystalline anisotropy in this compound. In a field of 50 kOe the magnetization reaches a value of 28.4 emu/g. Assuming that our measurements performed on a polycrystalline specimen represent the response of a randomly oriented fixed powder, the latter value of σ yields the cerium ordered magnetic moment of $3.09\mu_B$ or $1.96\mu_B$ in the case of uniaxial or easy-plane anisotropy, respectively. Whereas the first value must be rejected as being unphysically large for a cerium compound, the latter one is close to $gJ=2.14$ expected for a free Ce^{3+} ion. Thus, it seems likely that the anisotropy in $\text{Ce}_2\text{Pd}_2\text{In}$ is of the easy-plane type. However, we are aware that the values of μ_{ord} derived above may be seriously overestimated because of a possible texture in the

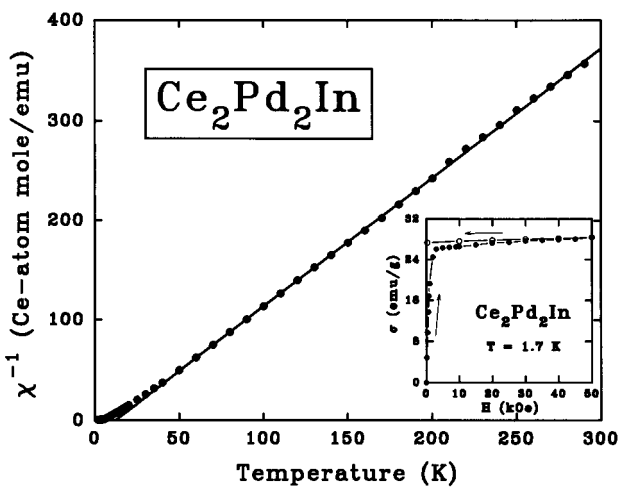


FIG. 7. Temperature variation of the inverse magnetic susceptibility for $\text{Ce}_2\text{Pd}_2\text{In}$. The solid line is a fit of the experimental data to the Curie-Weiss law. The inset displays the field dependence of the magnetization for $\text{Ce}_2\text{Pd}_2\text{In}$ measured at 1.7 K with increasing (filled symbols) and decreasing (open symbols) magnetic field.

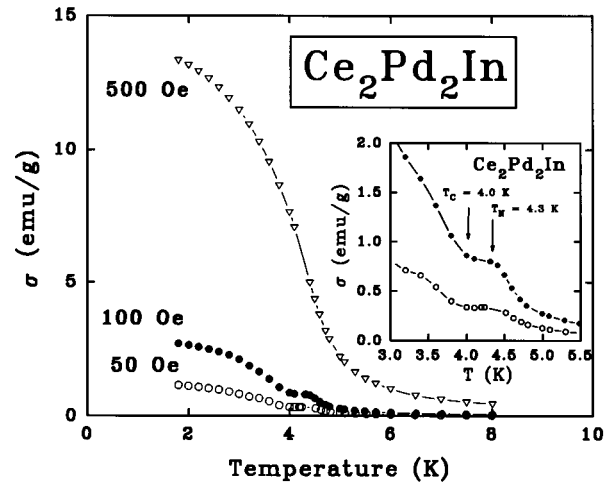


FIG. 8. Temperature dependence of the magnetization for $\text{Ce}_2\text{Pd}_2\text{In}$ measured in 50, 100, and 500 Oe. The inset shows $\sigma(T)$ in the vicinity of the magnetic phase transitions. The arrows mark the ordering temperatures.

bulk samples measured. Therefore, before drawing any further conclusions on the crystal-field ground state in $\text{Ce}_2\text{Pd}_2\text{In}$, detailed magnetization measurements of a single crystal of this compound (or at least a couple of free- and fixed-powder experiments⁴) are required.

In Fig. 8 are shown the magnetization vs temperature curves taken for $\text{Ce}_2\text{Pd}_2\text{In}$ in weak magnetic fields. These measurements revealed unexpectedly the presence of a small maximum in $\sigma(T)$ which is located just above the ferromagnetic region and could be associated with some rearrangement of cerium magnetic moments. It seems likely that this ternary cerium compound may exhibit more complex magnetic behavior undergoing first an antiferromagnetic phase transition at $T_N=4.3$ K and then becoming ferromagnetic below $T_c=4.0$ K. This suggestion has recently been corroborated in an independent investigation of $\text{Ce}_2\text{Pd}_2\text{In}$ by Hilscher *et al.*³³ who found a double-peak behavior in the temperature variation of the ac magnetic susceptibility. On the other hand, taking into account an extensive homogeneity range reported for this compound by Gordon *et al.*,¹⁶ an extrinsic nature of the anomaly at 4.3 K cannot be completely excluded at the present stage of our study. A neutron-diffraction experiment is in progress to clarify the origin of the observed feature.

In the temperature range 50–300 K the susceptibility of $\text{Ce}_2\text{Pd}_2\text{In}$ can be approximated by a Curie-Weiss law with the parameters: $\mu_{\text{eff}}=2.49\mu_B/\text{Ce atom}$ and $\theta_p=+12.3$ K (see Fig. 7). The positive value of the paramagnetic Curie temperature reflects ferromagnetic exchange interactions in this compound. Below 50 K a deviation of $\chi^{-1}(T)$ from a straight-line behavior occurs, likely due to crystal-field effects.

C. Electrical resistivity

$\text{Ce}_2\text{Ni}_2\text{In}$ and $\text{Ce}_2\text{Rh}_2\text{In}$

The electrical transport behavior of $\text{Ce}_2\text{Ni}_2\text{In}$ and $\text{Ce}_2\text{Rh}_2\text{In}$ is displayed in Fig. 9. The resistivity for both compounds varies with temperature in a manner characteristic of

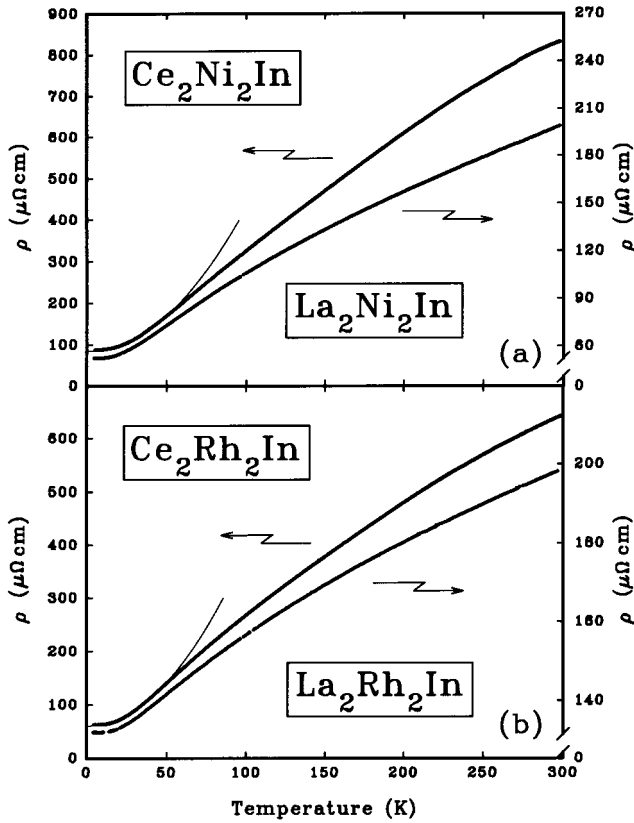


FIG. 9. Temperature dependence of the electrical resistivity for (a) $\text{Ce}_2\text{Ni}_2\text{In}$ and $\text{La}_2\text{Ni}_2\text{In}$ and (b) $\text{Ce}_2\text{Rh}_2\text{In}$ and $\text{La}_2\text{Rh}_2\text{In}$. The solid lines mark a T^2 variation of the resistivity of $\text{Ce}_2\text{Ni}_2\text{In}$ and $\text{Ce}_2\text{Rh}_2\text{In}$ at low temperatures.

nonmagnetic metals. Indeed, in respect to their overall shape these two $\rho(T)$ curves are very similar to the resistivity vs temperature dependences determined for the lanthanum-based counterparts $\text{La}_2\text{Ni}_2\text{In}$ and $\text{La}_2\text{Rh}_2\text{In}$ (see also Fig. 9). The residual resistivity ratio (RRR) = $\rho(300\text{ K})/\rho(4.5\text{ K})$ amounts to about 9 and 12 for $\text{Ce}_2\text{Ni}_2\text{In}$ and $\text{Ce}_2\text{Rh}_2\text{In}$, respectively. These numbers are rather satisfactory taking into account that the measurements were performed on unannealed polycrystalline samples. Yet, the absolute values of the resistivity for both compounds are very high. This is surely due to brittleness of the specimens measured which contained many macroscopic cracks. Surprisingly, annealing of the samples resulted in some enlargement in the magnitude of the resistivity likely because of creation of new internal cracks. Therefore, we present in Fig. 9 only the data obtained for the as-cast specimens but the values of ρ given in these figures must be taken as an upper bound of the real bulk resistivity of $\text{Ce}_2\text{Ni}_2\text{In}$ and $\text{Ce}_2\text{Rh}_2\text{In}$.

The $\rho(T)$ curves observed for $\text{Ce}_2\text{Ni}_2\text{In}$ and $\text{Ce}_2\text{Rh}_2\text{In}$ are reminiscent of the behavior of intermediate-valence materials.³⁴ According to the paramagnon picture of such systems their resistivity at low temperatures should reveal a T^2 dependence characteristic of a Fermi liquid.²⁹ Indeed, as shown by solid lines in Fig. 9, the resistivity of $\text{Ce}_2\text{Ni}_2\text{In}$ and $\text{Ce}_2\text{Rh}_2\text{In}$ can be well described below about 50 K by the expression

$$\rho(T) = \rho_0 + AT^2, \quad (7)$$

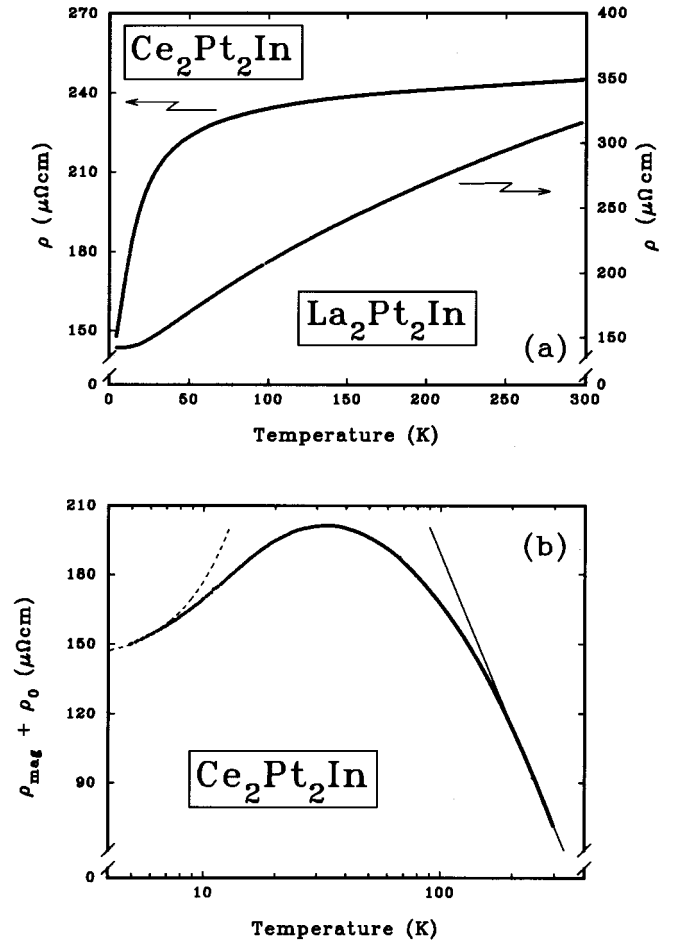


FIG. 10. (a) Temperature dependence of the electrical resistivity for $\text{Ce}_2\text{Pt}_2\text{In}$ and $\text{La}_2\text{Pt}_2\text{In}$. (b) Temperature-dependent magnetic contribution to the total electrical resistivity of $\text{Ce}_2\text{Pt}_2\text{In}$ (enlarged by the residual resistivity) shown in a semilogarithmic scale. The dashed line marks a T^2 variation of the resistivity at low temperatures, and the solid line is a least-squares fit to the Kondo formula (see text).

with the parameters $\rho_0 = 88\ \mu\Omega\text{cm}$ and $A = 0.018\ \mu\Omega\text{cm/K}^2$ for the former compound and $\rho_0 = 53\ \mu\Omega\text{cm}$ and $A = 0.022\ \mu\Omega\text{cm/K}^2$ for the latter compound, respectively. It is worthwhile to remind at this place that in the same temperature region also the magnetic susceptibility of these two intermetallics follows the paramagnon model (see Sec. III B). Unfortunately, the uncertainty in the absolute values of the resistivity hampered any further quantitative discussion of the electrical behavior in $\text{Ce}_2\text{Ni}_2\text{In}$ and $\text{Ce}_2\text{Rh}_2\text{In}$.

$\text{Ce}_2\text{Pt}_2\text{In}$

The temperature-dependent electrical resistivity of $\text{Ce}_2\text{Pt}_2\text{In}$ is shown in Fig. 10(a). This $\rho(T)$ curve strongly resembles the behavior of intermetallic compounds exhibiting spin fluctuations due to Kondo interactions,³⁵ for example, well-known heavy-fermion systems UPt_3 ,³⁶ UNi_2Al_3 ,³⁷ or many rare-earth and actinoid Laves phases³⁸ with an archetypal spin-fluctuator UAl_2 .³⁹ The resistivity shows first a pronounced rise at low temperatures which is followed by a saturation in the high-temperature region. At

TABLE III. Parameters of the fits of the resistivity for La_2T_2In compounds to the modified Bloch-Grüneisen expression [for the legend see Eq. (8) and the text].

Compound	ρ_0 ($\mu\Omega$ cm)	Θ_D (K)	R ($\mu\Omega$ cm/K)	K (10^{-7} $\mu\Omega$ cm/K ³)
$\text{La}_2\text{Ni}_2\text{In}$	52.5	118	0.578	9.9
$\text{La}_2\text{Cu}_2\text{In}$	25.9	114	0.413	6.1
$\text{La}_2\text{Rh}_2\text{In}$	32.0	119	0.268	5.1
$\text{La}_2\text{Pd}_2\text{In}$	91.8	130	0.964	12.5
$\text{La}_2\text{Pt}_2\text{In}$	42.4	104	0.707	14.3
$\text{La}_2\text{Au}_2\text{In}$	20.7	98	0.376	8.7

room temperature it amounts to about 245 $\mu\Omega$ cm, a value rather standard for narrow f -band materials.

In contrary, the lanthanum-based compound $\text{La}_2\text{Pt}_2\text{In}$ exhibits a metallic-type electrical behavior [see Fig. 10(a)] but with some negative curvature for $\rho(T)$ at elevated temperatures. Based on the Matthiessen's rule, the resistivity of this nonmagnetic compound can be described by the modified Bloch-Grüneisen relation^{40,41}

$$\rho(T) = \rho_0 + 4R\Theta_D \left(\frac{T}{\Theta_D} \right)^5 \int_0^{\Theta_D/T} \frac{x^5 dx}{(e^x - 1)(1 - e^{-x})} - KT^3, \quad (8)$$

where ρ_0 is the temperature-independent residual resistivity, the second term accounts for the electron-phonon scattering processes, and a T^3 contribution is due to scattering of the conduction electrons into a narrow d band. Consequently, the temperature-independent coefficients R and K in Eq. (8) are directly related to the strength of the electron-phonon and the s - d interactions, respectively, whereas the symbol Θ_D stands for the Debye temperature. The values of ρ_0 , Θ_D , R , and K , derived for $\text{La}_2\text{Pt}_2\text{In}$ by least-squares fitting procedure, are given in Table III.

Assuming that the resistivity of the lanthanum-based counterpart can be taken as a good approximation of the phonon contribution to the total measured resistivity of $\text{Ce}_2\text{Pt}_2\text{In}$ we expressed $\rho(T)$ for this compound as follows:

$$\rho(T) = \rho_0 + \rho(\text{La}_2\text{Pt}_2\text{In}) - \rho_0(\text{La}_2\text{Pt}_2\text{In}) + \rho_{\text{mag}}(T) \quad (9)$$

and in this way extracted the temperature dependence of the magnetic scattering resistivity which is displayed in Fig. 10(b). Unfortunately, down to 4.5 K (the lower limit of our electrical measurements) $\rho(T)$ of $\text{Ce}_2\text{Pt}_2\text{In}$ does not show any tendency for saturation and hence we cannot determine the residual resistivity ρ_0 and in the further analysis are forced to consider the sum $\rho_0 + \rho_{\text{mag}}(T)$. Nevertheless, it is apparent from Fig. 10(b) that at elevated temperatures the magnetic contribution to the resistivity of $\text{Ce}_2\text{Pt}_2\text{In}$ exhibits a pronounced logarithmic decrease with rising temperature which could be ascribed to the hallmark of Kondo-type interactions of the conduction electrons with the localized cerium magnetic moments. The fit of $\rho_{\text{mag}}(T)$ (for $T > 200$ K) to the standard formula⁴²

$$\rho_{\text{mag}}(T) = \rho_0^\infty - c_K \ln(T) \quad (10)$$

yielded a value of 685 $\mu\Omega$ cm for the sum of ρ_0 and the spin-disorder resistivity ρ_0^∞ and a value of 248 $\mu\Omega$ cm for the Kondo coefficient c_K . In the scope of the theory by Kondo,⁴² c_K is proportional to the electronic density of states at the Fermi energy $N(E_F)$. Thus, the quite large value of the Kondo coefficient derived for $\text{Ce}_2\text{Pt}_2\text{In}$ may indicate strongly enhanced $N(E_F)$ making this compound a good candidate for a heavy-fermion research.

On the other hand, it is well known⁴³ that the electronic ground state of dense Kondo systems is a heavy-Fermi liquid, and hence their electrical resistivity should vary at low temperatures according to Eq. (7) where the coefficient A in the T^2 term is inversely proportional to the square of the Kondo temperature T_K .⁴⁴ Moreover, according to the scaling found by Kadowaki and Woods⁴⁵ for established heavy-fermion compounds, the constant A is related to the electronic coefficient of the specific heat γ via the universal ratio

$$A/\gamma^2 = 1.0 \times 10^{-5} \mu\Omega \text{ cm K}^2 \text{ mole}^2/\text{mJ}^2. \quad (11)$$

Unfortunately, as shown by the dashed line in Fig. 10(b), the resistivity of $\text{Ce}_2\text{Pt}_2\text{In}$ shows a T^2 dependence only in a very limited temperature range namely up to about 7 K. The parameter A is equal here to 0.38 $\mu\Omega$ cm/K² thus yielding from Eq. (11) a rather small γ value of about 190 mJ/mole K². However, this latter value is obviously only a very rough estimate of γ and any reliable conclusion about the ground state in $\text{Ce}_2\text{Pt}_2\text{In}$ unconditionally requires an extension of resistivity studies to lower temperatures. Moreover, specific-heat measurements of $\text{Ce}_2\text{Pt}_2\text{In}$ are in progress at the time being and they are expected to shed more light on the low-temperature electronic properties of this intriguing material. Finally, it is noteworthy that the uranium-based counterpart to the compound discussed, i.e., $\text{U}_2\text{Pt}_2\text{In}$, exhibits a γ value as high as 830 mJ/mole K² (Ref. 5) which undoubtedly places it well amidst heavy-fermion systems.

$\text{Ce}_2\text{Cu}_2\text{In}$, $\text{Ce}_2\text{Au}_2\text{In}$ and $\text{Ce}_2\text{Pd}_2\text{In}$

The results of electrical measurements for $\text{Ce}_2\text{Cu}_2\text{In}$, $\text{Ce}_2\text{Au}_2\text{In}$, and $\text{Ce}_2\text{Pd}_2\text{In}$ are presented in Figs. 11(a), 12(a), and 13(a), respectively. The $\rho(T)$ dependences clearly reflect a metallic character of all the three materials studied. The magnitude of the room-temperature resistivity for the Cu- and Au-containing compounds is similar to that of $\text{Ce}_2\text{Pt}_2\text{In}$. In contrast, the value of $\rho(300$ K) measured for $\text{Ce}_2\text{Pd}_2\text{In}$ is much larger probably due to a high concentration in the sample of internal cracks. It is, however, noteworthy that measuring the same specimen several times we found a rather good reproducibility of its $\rho(T)$ with no discontinuities or any appreciable hysteresis in the data. Alike in the case of $\text{Ce}_2\text{Ni}_2\text{In}$ and $\text{Ce}_2\text{Rh}_2\text{In}$, annealing of the palladium-containing compound did not bring any significant improvement in the RRR ratio nor significant changes in the absolute values of the resistivity.

The overall shape of the $\rho(T)$ variations found for $\text{Ce}_2\text{Cu}_2\text{In}$, $\text{Ce}_2\text{Au}_2\text{In}$, and $\text{Ce}_2\text{Pd}_2\text{In}$ appears to be typical for magnetically ordered intermetallics exhibiting a combined effect of the Kondo and crystal-field interactions. The resistivity decreases first smoothly with decreasing temperature, then goes through a broad knee around 100 K where it starts to drop off faster, and finally shows a shallow minimum

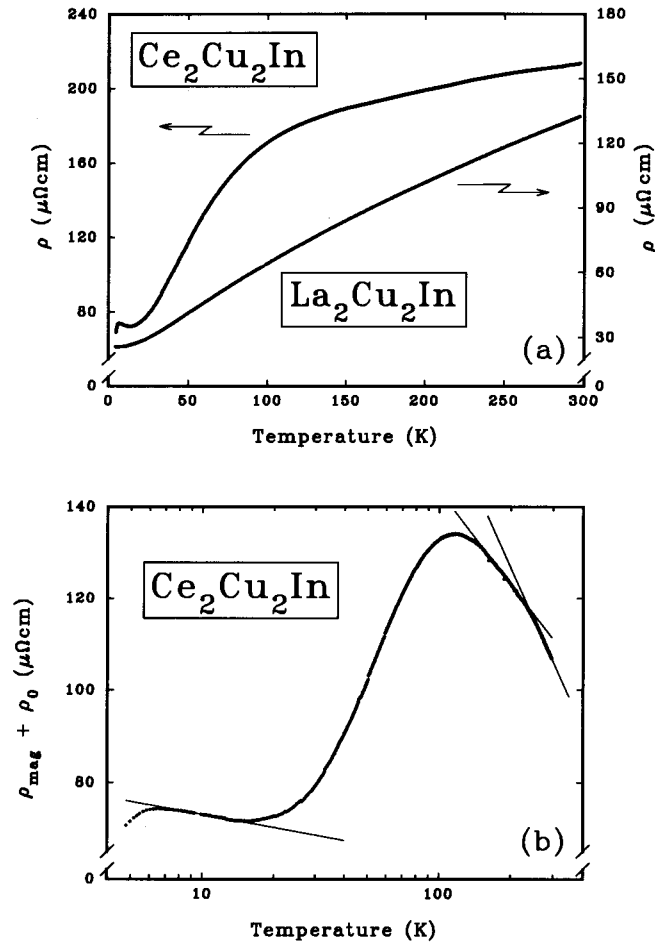


FIG. 11. (a) Temperature dependence of the electrical resistivity for $\text{Ce}_2\text{Cu}_2\text{In}$ and $\text{La}_2\text{Cu}_2\text{In}$. (b) Temperature-dependent magnetic contribution to the total electrical resistivity of $\text{Ce}_2\text{Cu}_2\text{In}$ (enlarged by the residual resistivity) shown in a semilogarithmic scale. The solid lines are least-squares fits of $\rho(T)$ to the Kondo formula (see text).

which is followed for $\text{Ce}_2\text{Cu}_2\text{In}$ and $\text{Ce}_2\text{Pd}_2\text{In}$ by an abrupt change in the slope near the magnetic phase transition. This latter anomaly can be ascribed to a strong reduction in scattering of the conduction electrons due to the onset of magnetic order. The temperature region studied ($T > 4.5$ K) did not allow us to observe any similar low-temperature drop in the resistivity of $\text{Ce}_2\text{Au}_2\text{In}$ for which $T_N = 3.2$ K.

In order to separate the magnetic contributions from the total resistivity of $\text{Ce}_2\text{Cu}_2\text{In}$, $\text{Ce}_2\text{Au}_2\text{In}$, and $\text{Ce}_2\text{Pd}_2\text{In}$ electrical measurements of their nonmagnetic counterparts, $\text{La}_2\text{Cu}_2\text{In}$, $\text{La}_2\text{Au}_2\text{In}$, and $\text{La}_2\text{Pd}_2\text{In}$, were performed. The results of these studies are displayed in Figs. 11–13. It appears that all the lanthanum-based compounds exhibit a metallic type of the electrical conductivity. Thus, their $\rho(T)$ variations were analyzed in terms of the modified Bloch-Grüneisen model,^{40,41} and the parameters of the successful least-squares fits of the experimental data to Eq. (8) are listed in Table III. Subsequently, in a similar manner as for $\text{Ce}_2\text{Pt}_2\text{In}$ [see Eq. (9)], the temperature variations of the magnetic scattering resistivity for $\text{Ce}_2\text{Cu}_2\text{In}$, $\text{Ce}_2\text{Au}_2\text{In}$, and $\text{Ce}_2\text{Pd}_2\text{In}$ have been derived. The so-obtained $\rho_{\text{mag}}(T)$ curves (enlarged in each case by the residual resistivity ρ_0) are shown in a semilogarithmic representation in Figs. 11(b),

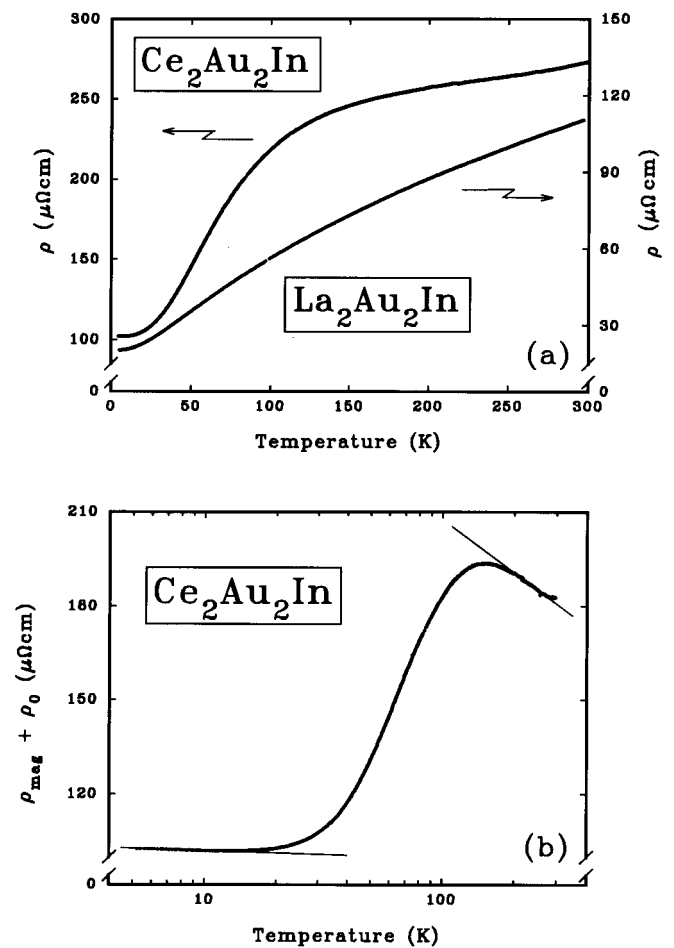


FIG. 12. (a) Temperature dependence of the electrical resistivity for $\text{Ce}_2\text{Au}_2\text{In}$ and $\text{La}_2\text{Au}_2\text{In}$. (b) Temperature-dependent magnetic contribution to the total electrical resistivity of $\text{Ce}_2\text{Au}_2\text{In}$ (enlarged by the residual resistivity) shown in a semilogarithmic scale. The solid lines are least-squares fits of $\rho(T)$ to the Kondo formula (see text).

12(b), and 13(b), respectively. Characteristic maxima and regions of the logarithmic decrease in $\rho_{\text{mag}}(T)$ seen in these figures seem to corroborate our hypothesis of an interplay of Kondo and crystal-field interactions. The low-temperature maximum could be associated with the Kondo temperature that would be of about 6 K for both $\text{Ce}_2\text{Cu}_2\text{In}$ and $\text{Ce}_2\text{Pd}_2\text{In}$ but lower than 4.5 K in the case of $\text{Ce}_2\text{Au}_2\text{In}$. Alternatively, these maxima in $\rho_{\text{mag}}(T)$ may be due to short-range interactions. In turn, the maxima seen at high temperatures are likely a result from Kondo scattering in the presence of crystal-field effects.

The regions of $-\ln(T)$ dependences of the resistivity were analyzed in terms of the Kondo theory.⁴² As seen from Fig. 11(b), as many as three different logarithmic slopes of $\rho_{\text{mag}}(T)$ can be identified for $\text{Ce}_2\text{Cu}_2\text{In}$ and the fits of this resistivity behavior to Eq. (10) yield the following parameters: $(\rho_0^\infty + \rho_0)^{(1)} = 82.4 \mu\Omega\text{cm}$ and $c_K^{(1)} = 9.4 \mu\Omega\text{cm}$ (for $9 \text{ K} < T < 12 \text{ K}$), $(\rho_0^\infty + \rho_0)^{(2)} = 279.2 \mu\Omega\text{cm}$ and $c_K^{(2)} = 49.9 \mu\Omega\text{cm}$ (for $160 \text{ K} < T < 230 \text{ K}$), $(\rho_0^\infty + \rho_0)^{(3)} = 393.6 \mu\Omega\text{cm}$ and $c_K^{(3)} = 115.9 \mu\Omega\text{cm}$ (for $T > 250 \text{ K}$). In the case of $\text{Ce}_2\text{Au}_2\text{In}$ there are two regions of the logarithmic variations of the resistivity [see Fig. 12(b)]. For $6 \text{ K} < T < 10 \text{ K}$ the following values have been found: $(\rho_0^\infty + \rho_0)^{(1)} = 104.6 \mu\Omega\text{cm}$

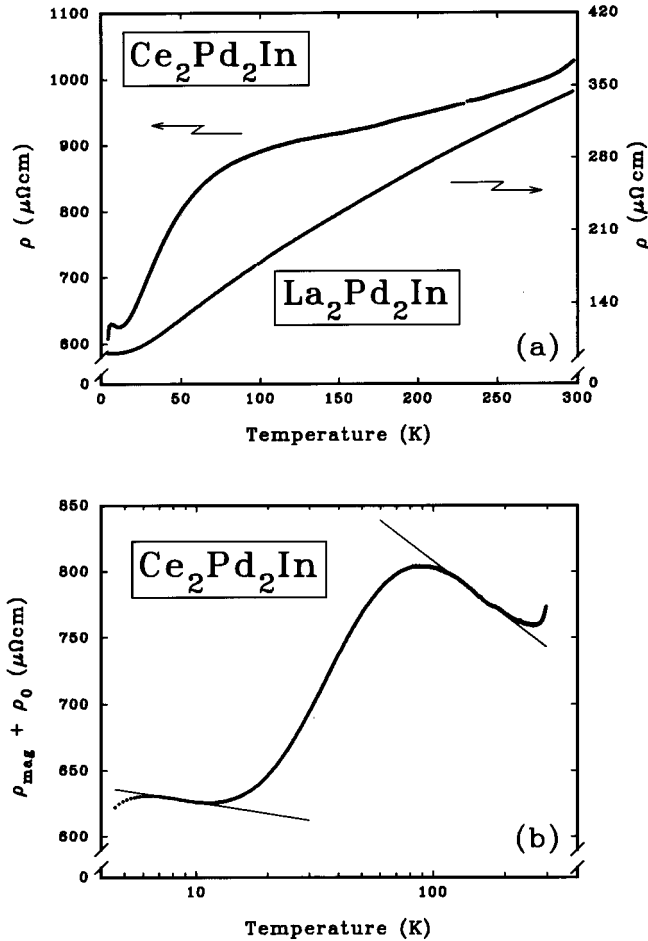


FIG. 13. (a) Temperature dependence of the electrical resistivity for $\text{Ce}_2\text{Pd}_2\text{In}$ and $\text{La}_2\text{Pd}_2\text{In}$. (b) Temperature-dependent magnetic contribution to the total electrical resistivity of $\text{Ce}_2\text{Pd}_2\text{In}$ (enlarged by the residual resistivity) shown in a semilogarithmic scale. The solid lines are least-squares fits of $\rho(T)$ to the Kondo formula (see text).

and $c_K^{(1)} = 2.4 \mu\Omega \text{ cm}$, and for the range $200 \text{ K} < T < 260 \text{ K}$ the parameters are $(\rho_0^\infty + \rho_0)^{(2)} = 320.0 \mu\Omega \text{ cm}$ and $c_K^{(2)} = 56.2 \mu\Omega \text{ cm}$. Finally, the same analysis of the $\rho_{\text{mag}}(T) + \rho_0$ variation observed for $\text{Ce}_2\text{Pd}_2\text{In}$ [see Fig. 13(b)] gave the following results: $(\rho_0^\infty + \rho_0)^{(1)} = 654.6 \mu\Omega \text{ cm}$ and $c_K^{(1)} = 28.5 \mu\Omega \text{ cm}$ in the temperature range $7 \text{ K} < T < 10 \text{ K}$ and $(\rho_0^\infty + \rho_0)^{(2)} = 1083.6 \mu\Omega \text{ cm}$, $c_K^{(2)} = 137.7 \mu\Omega \text{ cm}$ for $130 \text{ K} < T < 200 \text{ K}$.

According to the theory developed by Cornut and Coqblin,⁴⁶ the combined influence of the Kondo effect and the crystal-field interactions on the electrical properties of a cerium intermetallic compound results in the magnetic contribution to the total resistivity which can be expressed as

$$\rho_{\text{mag}}(T) = \alpha J^2 \frac{\lambda_i^2 - 1}{\lambda_i(2j+1)} + 2\alpha N(E_F) J^3 \frac{\lambda_i^2 - 1}{2j+1} \ln\left(\frac{T}{D_i}\right). \quad (12)$$

The symbol J denotes here the negative s - f exchange integral, λ_i stands for the effective degeneracy of the crystal field $4f$ level, a is a constant and D_i is the effective cutoff parameter for a given crystal-field state. From Eq. (12) it becomes clear that the ratio of the logarithmic slopes of the high- and low-temperature resistivities is determined only by

the effective degeneracies of crystal-field levels λ_i . In the case of Ce^{3+} ions experiencing a tetragonal crystal-field potential, the six-fold degenerated ground multiplet ${}^2F_{5/2}$ is split into three doublets. Therefore, for well separated crystal-field levels one can expect three regions of a $-\ln(T)$ variation of the resistivity. The slopes of these three curves give according to Eq. (12) the following ratios: 3:15 (ground doublet–pseudoquartet), 3:35 (ground doublet–pseudo-octet), and 15:35 (pseudoquartet–pseudosextet).

Interestingly, the $c_K^{(i)}$ coefficients derived for $\text{Ce}_2\text{Cu}_2\text{In}$ nicely fulfill the above predictions. Hence, we can conclude that the first excited doublet in this compound lies probably about 120 K above the ground state [position of the maximum in $\rho_{\text{mag}}(T)$] and the total crystal-field splitting may be of the order of 250 K, i.e., at the temperature where the change in slope of $-\ln(T)$ occurs. For $\text{Ce}_2\text{Pd}_2\text{In}$ the ratio of the Kondo coefficients is close to that expected for the system of two lowest lying doublets being separated in energy by about 90 K [see Fig. 13(b)]. The rise in ρ_{mag} observed for this compound above 270 K could be consequently interpreted as the onset of substantial population of the highest crystal-field state. Thus, the total splitting in $\text{Ce}_2\text{Pd}_2\text{In}$ would be larger than 300 K. In contrast to the previous two compounds, for $\text{Ce}_2\text{Au}_2\text{In}$ no agreement with theory can be found as the $c_K^{(1)}/c_K^{(2)}$ ratio is much smaller than that derived from Eq. (12). Yet, even in this case it seems likely that the position of the maximum in $\rho_{\text{mag}}(T)$ may be associated with the crystal-field splitting in this compound of about 150 K. It is possible that, in a similar manner as in $\text{Ce}_2\text{Pd}_2\text{In}$, a small increase in the magnetic scattering seen above 260 K reflects the presence of the highest doublet which is only poorly occupied at $T < 300 \text{ K}$.

IV. SUMMARY

The distinct changes in the unit-cell volumes observed within the $\text{Ce}_2\text{T}_2\text{In}$ series cannot be fully accounted for by considering the T -metal atomic sizes only. These effects have rather an electronic origin and result from specific electronic configuration of the constituent transition elements. In the case of $\text{Ce}_2\text{Ni}_2\text{In}$ and $\text{Ce}_2\text{Rh}_2\text{In}$ each transition-metal atom supplies two d holes. The Ce- T distances in these compounds are relatively short and both the $4f$ electrons of cerium and the d electrons of the transition metal effectively contribute to bonding. Due to the f - d hybridization a broadened f band is pinned at the Fermi energy allowing, by this means, charge fluctuations between different electronic states of the cerium atom. As a result both the compounds reveal features characteristic of intermediate valence systems. In contrast, all the remaining $\text{Ce}_2\text{T}_2\text{In}$ ternaries studied exhibit well localized magnetism due to the presence of stable Ce^{3+} ions. The compounds containing transition elements with completely filled d band, i.e., $\text{Ce}_2\text{Cu}_2\text{In}$, $\text{Ce}_2\text{Pd}_2\text{In}$, and $\text{Ce}_2\text{Au}_2\text{In}$, order magnetically at low temperatures. Their electrical behavior is dominated by an interplay of strong Kondo and crystal-field interactions. The f - d hybridization effects are in these phases rather weak if any. A particularly interesting case represents here $\text{Ce}_2\text{Pt}_2\text{In}$. Taking into account the electronic configuration of the platinum metal with one d hole in its $5d$ band it seems likely that some f - d hybridization does occur in this ternary compound. Indeed,

although $\text{Ce}_2\text{Pt}_2\text{In}$ exhibits all the features characteristic of well localized magnetic systems, it does not order magnetically and remains paramagnetic down to the lowest temperatures examined. It appears that $\text{Ce}_2\text{Pt}_2\text{In}$ can be located in between the two limits represented on one side by nonmagnetic $\text{Ce}_2\text{Ni}_2\text{In}$ and $\text{Ce}_2\text{Rh}_2\text{In}$ and on the other side by magnetically ordered $\text{Ce}_2\text{Cu}_2\text{In}$, $\text{Ce}_2\text{Pd}_2\text{In}$, and $\text{Ce}_2\text{Au}_2\text{In}$. Due to this special position $\text{Ce}_2\text{Pt}_2\text{In}$ seems to be a good candidate for a heavy-fermion research.

ACKNOWLEDGMENTS

D. K. is indebted to the Austrian Science Foundation (FWF) for a Lise-Meitner stipend (Project No. M00122-CHE). Part of this research has been supported by FWF-Grant No. P8218. We are grateful to M. Vybornov for collecting the D5000 x-ray data and to Professor E. Bauer for many helpful discussions.

- ¹F. Mirambet, P. Gravereau, B. Chevalier, L. Trut, and J. Etourneau, *J. Alloys Compounds* **191**, L1 (1993).
- ²M. N. Peron, Y. Kergadallan, J. Rebizant, D. Meyer, J. M. Winand, S. Zwirner, L. Havela, H. Nakotte, J. C. Spirlet, G. M. Kalvius, E. Colineau, J. L. Oddou, C. Jeandey, and J. P. Sanchez, *J. Alloys Compounds* **201**, 203 (1994).
- ³F. Mirambet, B. Chevalier, L. Fournès, P. Gravereau, and J. Etourneau, *J. Alloys Compounds* **203**, 29 (1994).
- ⁴H. Nakotte, K. Prokeš, E. Brück, N. Tang, F. R. de Boer, P. Svoboda, V. Sechovský, L. Havela, J. M. Winand, A. Seret, J. Rebizant, and J. C. Spirlet, *Physica B* **201**, 247 (1994).
- ⁵L. Havela, V. Sechovský, P. Svoboda, M. Diviš, H. Nakotte, K. Prokeš, F. R. de Boer, A. Purwanto, R. A. Robinson, A. Seret, J. M. Winand, J. Rebizant, J. C. Spirlet, M. Richter, and H. Eschrig, *J. Appl. Phys.* **76**, 6214 (1994).
- ⁶A. Purwanto, R. A. Robinson, L. Havela, V. Sechovský, P. Svoboda, H. Nakotte, K. Prokeš, F. R. de Boer, A. Seret, J. M. Winand, J. Rebizant, and J. C. Spirlet, *Phys. Rev. B* **50**, 6792 (1994).
- ⁷H. Nakotte, A. Purwanto, R. A. Robinson, K. Prokeš, J. C. P. Klaasse, P. F. de Châtel, F. R. de Boer, L. Havela, V. Sechovský, L. C. J. Pereira, A. Seret, J. Rebizant, J. C. Spirlet, and F. Trouw, *Phys. Rev. B* **53**, 3263 (1996).
- ⁸J. P. Sanchez, E. Colineau, C. Jeandey, L. L. Oddou, J. Rebizant, A. Seret, and J. C. Spirlet, *Physica B* **206&207**, 531 (1995).
- ⁹M. Diviš, M. Richter, and H. Eschrig, *Solid State Commun.* **90**, 99 (1994).
- ¹⁰M. Diviš, M. Olšovec, M. Richter, and H. Eschrig, *J. Magn. Magn. Mater.* **140-144**, 1365 (1995).
- ¹¹K. Prokeš, E. Brück, H. Nakotte, P. F. de Châtel, and F. R. de Boer, *Physica B* **206&207**, 8 (1995).
- ¹²S. F. Matar, *J. Magn. Magn. Mater.* **151**, 263 (1995).
- ¹³L. Havela, V. Sechovský, P. Svoboda, H. Nakotte, K. Prokeš, F. R. de Boer, A. Seret, J. M. Winand, J. Rebizant, J. C. Spirlet, A. Purwanto, and R. A. Robinson, *J. Magn. Magn. Mater.* **140-144**, 1367 (1995).
- ¹⁴Ya. M. Kalychak, V. I. Zaremba, V. M. Baranyak, P. Yu. Zavali, V. A. Bruskov, L. V. Sysa, and O. V. Dmytrakh, *Inorg. Mater.* **26**, 94 (1990).
- ¹⁵F. Hulliger and B. Z. Xue, *J. Alloys Compounds* **215**, 267 (1994).
- ¹⁶R. A. Gordon, Y. Ijiri, C. M. Spencer, and F. J. DiSalvo, *J. Alloys Compounds* **224**, 101 (1995).
- ¹⁷F. Hulliger, *J. Alloys Compounds* **217**, 164 (1995).
- ¹⁸F. Hulliger, *J. Alloys Compounds* **221**, L11 (1995).
- ¹⁹K. Yvon, W. Jeitschko, and E. Parthé, *J. Appl. Crystallogr.* **10**, 73 (1977).
- ²⁰R. Pöttgen, *Z. Naturforsch.* **49b**, 1309 (1994).
- ²¹R. Pöttgen, *Z. Naturforsch.* **49b**, 1525 (1994).
- ²²P. Gravereau, F. Mirambet, B. Chevalier, F. Weill, L. Fournès, D. Laffargue, and J. Etourneau (unpublished).
- ²³L. C. J. Pereira, J. M. Winand, F. Wastin, J. Rebizant, and J. C. Spirlet (unpublished).
- ²⁴G. Sheldrick, *SHELX, Program for Structure Determination*, University of Cambridge, 1976.
- ²⁵J. Rodriguez-Carvajal (unpublished).
- ²⁶E. Parthé and L. M. Gelato, *Acta Crystallogr. A* **40**, 169 (1984).
- ²⁷M. T. Béal-Monod and J. M. Lawrence, *Phys. Rev. B* **21**, 5400 (1980).
- ²⁸B. Chevalier, P. Rogl, K. Hiebl, and J. Etourneau, *J. Solid State Chem.* **107**, 327 (1993).
- ²⁹J. M. Lawrence, P. S. Riseborough, and R. D. Parks, *Rep. Prog. Phys.* **44**, 1 (1981).
- ³⁰B. C. Sales and D. K. Wohlleben, *Phys. Rev. Lett.* **35**, 1240 (1975).
- ³¹V. K. Pecharsky, K. A. Gschneider, Jr., and L. L. Miller, *Phys. Rev. B* **43**, 10 906 (1991).
- ³²J. Röhler, in *Handbook on the Physics and Chemistry of Rare Earths*, edited by K. A. Gschneider, Jr., L. Eyring, and S. Hüfner (North-Holland, Amsterdam, 1987), Vol. 10, p. 453.
- ³³G. Hilscher *et al.* (unpublished).
- ³⁴D. Wohlleben and B. Wittershagen, *Adv. Phys.* **34**, 403 (1985).
- ³⁵T. Moriya, *Spin Fluctuations in Itinerant Electron Magnetism* (Springer, Berlin, 1985).
- ³⁶M. S. Wire, J. D. Thompson, and Z. Fisk, *Phys. Rev. B* **30**, 5591 (1984).
- ³⁷C. Geibel, S. Thies, D. Kaczorowski, A. Mehner, A. Grauel, B. Seidel, U. Ahlheim, R. Helfrich, K. Petersen, C. D. Bredl, and F. Steglich, *Z. Phys. B* **83**, 305 (1991).
- ³⁸J. M. Fournier and E. Gratz, in *Handbook on the Physics and Chemistry of Rare Earths*, edited by K. A. Gschneider, Jr., L. Eyring, G. H. Lander, and G. R. Choppin (North-Holland, Amsterdam, 1993), Vol. 17, p. 409.
- ³⁹A. J. Arko, M. B. Brodsky, and W. J. Nellis, *Phys. Rev. B* **5**, 4564 (1972).
- ⁴⁰N. F. Mott and H. Jones, *The Theory of the Properties of Metals and Alloys* (Oxford University Press, London, 1958).
- ⁴¹G. Grimvall, *The Electron-Phonon Interaction in Metals* (North-Holland, Amsterdam, 1981).
- ⁴²J. Kondo, *Prog. Theor. Phys. Jpn.* **32**, 37 (1964).
- ⁴³D. Pines and P. Nozières, *The Theory of Quantum Liquids* (Addison-Wesley, New York, 1980).
- ⁴⁴K. H. Fischer, *Z. Phys. B* **74**, 475 (1989).
- ⁴⁵K. Kadowaki and S. B. Woods, *Solid State Commun.* **58**, 507 (1986).
- ⁴⁶D. Cornut and B. Coqblin, *Phys. Rev. B* **5**, 4541 (1972).